A second shell residue modulates a conserved ATP-binding site with radically different affinities for ATP

Alexander Krah [a,b,*,1], Bas van der Hoeven [c], Luuk Mestrom [c], Fabio Tonin [c], Kirsten C. C. Knobel [c], Peter J. Bond [b,d], Duncan G.G. McMillan [c,**,1]

[a] Department of Biophysics, Graduate School of Science, Kyoto University, Kitashirakawa-Oiwakecho, Sakyo-ku, Kyoto 606-8502, Japan
[b] Bioinformatics Institute, Agency for Science, Technology and Research (A*STAR), 30 Biopolis Str., #07-01 Matrix, 138671, Singapore
[c] Delft University of Technology, Department of Biotechnology, Van der Maasweg 9, Delft 2629HZ, the Netherlands
[d] National University of Singapore, Department of Biological Sciences, 14 Science Drive 4, 117543, Singapore

ABSTRACT

Background: Prediction of ligand binding and design of new function in enzymes is a time-consuming and expensive process. Crystallography gives the impression that proteins adopt a fixed shape, yet enzymes are functionally dynamic. Molecular dynamics offers the possibility of probing protein movement while predicting ligand binding. Accordingly, we choose the bacterial F_1F_o ATP synthase ε subunit to unravel why ATP affinity by ε subunits from *Bacillus subtilis* and *Bacillus* PS3 differs ~500-fold, despite sharing identical sequences at the ATP-binding site.
Methods: We first used the *Bacillus* PS3 ε subunit structure to model the *B. subtilis* ε subunit structure and used this to explore the utility of molecular dynamics (MD) simulations to predict the influence of residues outside the ATP binding site. To verify the MD predictions, point mutants were made and ATP binding studies were employed.
Results: MD simulations predicted that E102 in the *B. subtilis* ε subunit, outside of the ATP binding site, influences ATP binding affinity. Engineering E102 to alanine or arginine revealed a ~10 or ~54 fold increase in ATP binding, respectively, confirming the MD prediction that E102 drastically influences ATP binding affinity.
Conclusions: These findings reveal how MD can predict how changes in the "second shell" residues around substrate binding sites influence affinity in simple protein structures. Our results reveal why seemingly identical ε subunits in different ATP synthases have radically different ATP binding affinities.
General significance: This study may lead to greater utility of molecular dynamics as a tool for protein design and exploration of protein design and function.

1. Introduction

Protein interactions with their ligands, cofactors, DNA/RNA, and other proteins, are crucial for their function and regulation. It is well established that amino acid substitutions at a ligand/drug binding site can alter affinity or selectivity. This knowledge has been employed for decades in various guises, from directed evolution and site-directed mutagenesis for enzyme engineering in biocatalysis to natural biological systems where pathogens use natural selection to develop multi-drug resistance [1]. Comparison of homologous sequences in different species can help to understand ligand binding, as illustrated *e.g.* by the identification of the Walker A and Walker B ATP binding motifs across multiple protein classes such as ATP synthase, myosin, and kinases [2].

Understanding the effects of amino acid substitutions in homologous proteins from different organisms in the context of their three-dimensional structures is often crucial to rationalize the molecular

basis for ligand binding. This is typically aided by X-ray crystallography of apo and/or holo states [3–5], and may also be supported by NMR spectroscopy [6] or cryo-electron microscopy [7]. For example, the crystal and cryo-EM structures of the mycobacterial ATP synthase F_o rotor revealed special features of a binding site that has been proposed to govern efficacy of the antitubercular drug bedaquiline (BDQ, Sirturo; [8]),. In this context, the knowledge garnered enabled the development of structurally less complex and hence lower-cost antitubercular analogues [9], supporting the notion that understanding the molecular basis for ligand binding can facilitate the initial steps in rational drug design [10].

In addition, enzyme engineering can be used to change enzyme affinity. This is of particular interest in the fields of biocatalysis and biosensing. For example, cytochrome *c* has been used in place of traditional catalysts for creating carbon-silicon bonds, because traditional approaches require expensive trace metals. It noteworthy that mining trace

metals is not the green-chemistry approach required for a sustainable future. In this light of this, Kan et al. (2016) used directed evolution together with protein crystallography to engineer cytochrome *c* from *Rhodothermus marinus* to be 15-fold more efficient than current industrial catalysts [11]. In addition, in the biosensor field the *Bacillus* PS3 ATP synthase ε subunit has recently been engineered for use as an *in vivo* ATP biosensor [12].

However, despite the obvious utility of traditional approaches, methodologies such as crystallography and directed evolution are time-consuming and expensive processes. In addition, crystallography gives the false impression that a protein is a fixed, ridged entity, only showing the researcher a single conformation and not taking into account the physiological environment, yet enzymes are functionally dynamic entities. Taking BDQ as an example, the specificity of the interaction between the mycobacterial ATP synthase F_o rotor is still under investigation [13], and cross-talk effects in lipid environments have recently been identified [14]. To augment these limitations, a range of computational methods can be used to provide information complementary to structural and experimental studies [15] and can hence be used to predict binding sites for potential pharmacologically relevant targets and/or non-natural substrates to create value added products. Comparing known protein structures and ligand-protein interactions with related unknown protein structures can also help to understand pharmacological activities of currently used drugs [16,17]. Using

sequence and/or structural information, various bioinformatics methods can predict ligand binding sites and/or interactions *via* evolutionary, structural, geometric, or biophysical/biochemical properties [18–22]. Yet in many cases, these approaches have failed to reveal the reasons behind significant differences in ligand binding constants [23,24].

The MD simulation approach has "come of age" relatively recently in the context of accurately investigating the dynamics of ligand binding sites and receptor-drug interactions. For example, simulations have been used to predict ion binding to proteins [25,26], the presence of water molecules in the binding site [27], ligand-dependent conformational changes [28–32], the dynamics of cavities [33], and associated solvation [34]. It has been proposed that the Molecular Mechanics Poisson Boltzmann Surface Area (MM-PBSA) method can be used in an industrial drug development process to rapidly distinguish the binding affinities of different structurally similar uncharged ligands binding to a target [35].

Furthermore, free-energy calculations based on alchemical transformations within an MD simulation framework may be used to rigorously (but less rapidly) quantify ligand binding [36], or the binding selectivity [37], *e.g.* of purine-triphosphates towards a protein with 1000-fold greater affinity compared to the same protein [38].

The F-type ATP synthase is a membrane-bound enzyme complex that couples ATP synthesis at the F_1 head domain to trans-membrane proton flux through the F_o rotor. The activity of the complex may be regulated by several distinct mechanisms, which differ in mitochondria and
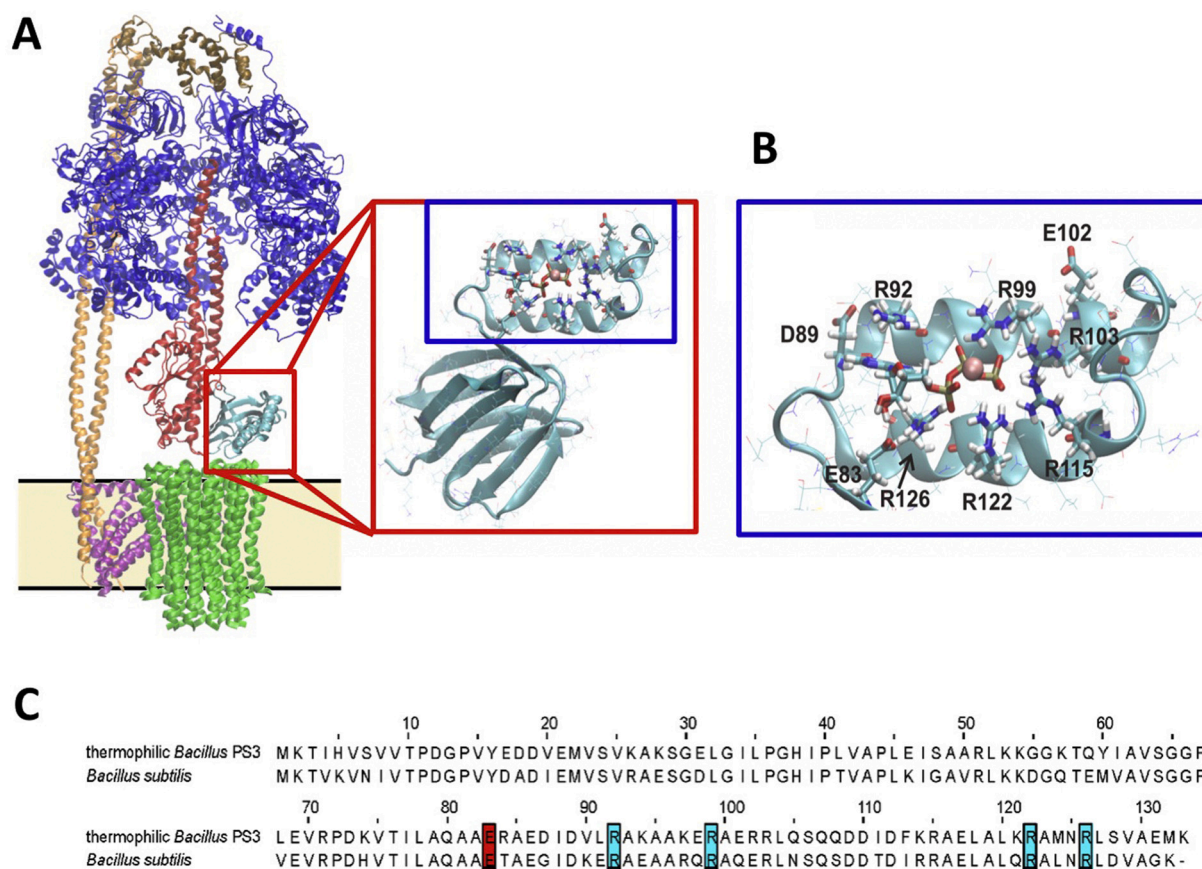

Fig. 1. ε subunit from *Bacillus subtilis*, its context in the ATP synthase structure, and an amino-acid comparison of the *B. subtilis* and *Bacillus* PS3 ε subunits. *A)* *Escherichia coli* F_1F_o multi-subunit complex protein is shown (PDB-ID: 5T4O), exchanging chain H with 1AQT) with ε subunit in the compact 'down-state' in which ATP is bound. The F_1 subunits, $\alpha_3\beta_3\gamma\delta\varepsilon$, are shown in blue, blue, red, brown and aqua respectively, and the membrane-bound F_o subunits, ab_2c_{10}, are shown in pink, yellow, and green respectively. Membrane boundaries around the F_o are indicated by a yellow box bound by black lines. The small red box encompasses the ε subunit, with the large red box being a magnified and detailed view of the *B. subtilis* ε subunit alone, with the blue boxed region being the ATP binding site (PDB-ID: 2E5Y and results of this study). *B)* Depicts an annotated magnification of the ATP binding site. ATP, potential ATP binding residues and E102 are highlighted in licorice. The Mg^{2+} ion coordinating ATP is shown in VdW spheres. *C)* Shows a partial alignment of the ε subunit from *B. subtilis* with that of *Bacillus* PS3. The ATP binding residues (E83, R92, R99, R122 and R126) are highlighted, with color indicating charge (red = negative; blue positive). (For interpretation of the references to colour in this figure legend, the reader is referred to the web version of this article.)

bacteria [39]. In most bacteria, the ε subunit inhibits the enzyme's catalytic activity in an ATP concentration-dependent manner to prevent wasteful hydrolysis of ATP [40]. This inhibition operates by virtue of a conformational change regulated by ATP binding/release at a binding site on its C-terminal domain, allosterically modulating the interaction of its N-terminal domain with the ATP synthase stalk (Fig. 1A and B).

Unfortunately, the full *Bacillus subtilis* F_1F_o ATP synthase structure has not yet been solved, and neither has the isolated epsilon subunit, but an *Escherichia coli* structure [41] has been used in Fig. 1A for the purpose of providing biological context. Interestingly, ATP binding affinities for the ε subunit from *B. subtilis* and *Bacillus* PS3 are 2.1 mM [23] and 4.3 μM [24] respectively, denoting a ~500 fold difference in affinity. Despite this, an alignment of their amino acid sequences and comparisons with available crystallographic [42] and biochemical [24] data suggest that the ATP binding site is completely conserved in both organisms. Because the ε subunit ATP binding site lies between two helices, it is also a simple prototype binding site to explore the utility of using MD simulations for enzyme engineering in fields such as biocatalysis to create enzymes with designed efficiencies towards industrially important products.

In this study, MD simulations based on a homology modeling using a known structure were used to predict the effects of a single point mutation, and subsequent biochemical experiments helped to reveal how the local environment in the vicinity of the ligand (ATP) binding site of the ε subunit from *B. subtilis* can drastically influence ATP binding affinity *via* subtle structural changes.

2. Results

2.1. MD simulations reveal different ATP binding sites in the ε subunits from thermophilic Bacillus PS3 and Bacillus subtilis

To elucidate why ATP binding affinity differs ~500-fold [23,24] between the *Bacillus subtilis* and *Bacillus* PS3, despite sharing an identical primary sequence ATP-binding site motif (Fig. 1C), we started by using an equilibrated homology model of the solved *Bacillus* PS3 ε subunit [42] and analyzed simulations of the ATP binding site structure in which a Mg^{2+} ion was modelled to ATP:Oα/Oβ. We used this approach because in this coordination, ATP has been found bound to the ε subunit (Fig. 1A and B) [43–45].
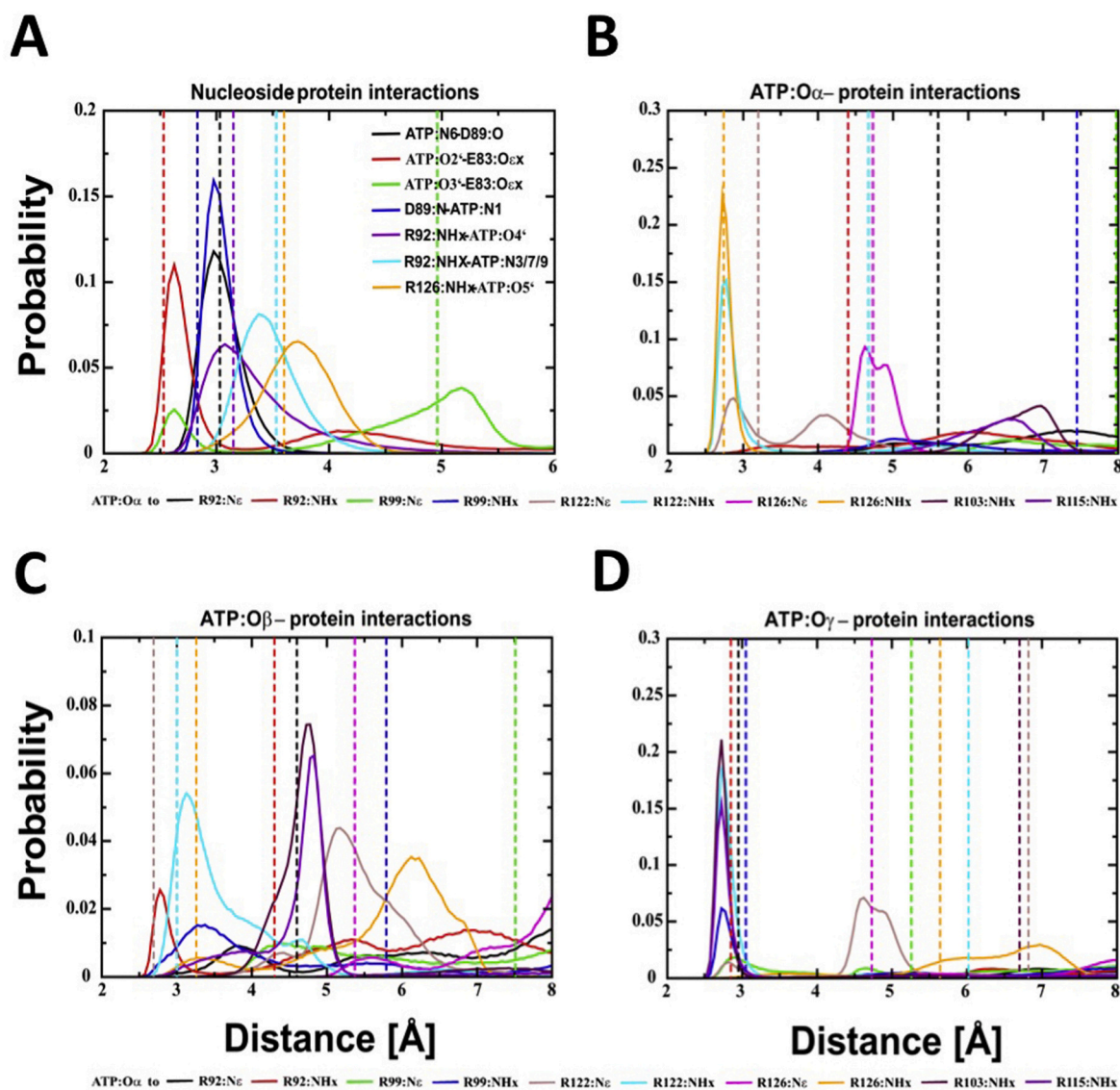

Fig. 2. Interactions of the protein with ATP in the ε subunit of *Bacillus subtilis*. A) Shows interactions with the nucleotide. In B), C) and D) histograms of relevant interactions with the ATP:Oα, ATP:Oβ and ATP:Oγ are shown, respectively. Data were derived from three independent runs, each comprising a 100 ns time period. Dashed lines indicate distances in the crystal structure of the ε subunit from *Bacillus* PS3 [42]. The timelines of relevant individual interactions are shown in Fig. S1.

From these simulations, we first measured the stability of the simulations as quality control (Figs. S2, S3). Furthermore, we calculated the distributions of binding site residues interacting with ATP (Fig. 2; timelines are shown in Fig. S1). The nucleoside is coordinated by hydrogen bonds with E83:Oε, D89:N, D89:O, R92:NHx (cation-π interactions with the adenosine ring) and a hydrogen bond to R126:NHx. The phosphate group is coordinated by R103:NHx, R115:NHx, R122:NHx and R126:NHx. This reflects a similar binding site composition to the nucleotide as the ε subunit from *Bacillus* PS3 [42,43]. However, a different binding site composition was found for binding the phosphate group in comparison to that in *Bacillus* PS3; the phosphate group is coordinated by R99 and not by R115. This prompted a closer examination of structurally neighboring residues, revealing that *Bacillus subtilis* has a glutamate residue (E102:Oεx; see Fig. 1C) which is not present in *Bacillus* PS3 (R102). Simulations suggest that E102 might sequester R99:NHx, preventing interaction with ATP and leading to the replacement of the R99:NHx - ATP:Oγ interaction with R103:NHx (Fig. 2). This notion is supported by previously reported gel filtration experiments, in which the R99A mutation caused a decreased ATP binding affinity [24].

2.2. In silico mutations suggest a profound influence of E102 on ATP binding site structure

To explore the hypothesis that E102 influences the ATP binding site structure, we decided to disrupt the E102-R99 interaction by introducing either a neutral (alanine) or repulsive (arginine) force in place of E102. It should be noted that the E102R mutation results in the same sequence motif (R102), as observed in the ε subunit from *Bacillus* PS3. Simulations were carried out on both *in silico* mutant ε subunits of *Bacillus subtilis*, revealing a stable protein structure (Fig. S2 and S3). Furthermore, we observed that the interaction of R99:NHx with ATP:Oγ was similar to that found in *Bacillus* PS3 (Fig. 3A), lending support to the notion that a single point mutation might result in a similar binding site structure, taking into account the remaining interactions (Fig. S4, S5 and S6).

We observed that R103 (both mutants) and R115 (E102A mutant) remain bound to ATP (Fig. S5 and S6), though this could in principle reflect a local energy minimum. The binding of R103 and R115 to ATP in the ε subunit from *B. subtilis* might be due to the limited simulation time, which does not allow the simulations to exit this local energy minimum, caused by attractive interactions (R103/R115 ➔ ATP:Oγ). The predicted binding sites of the WT ε subunits from *Bacillus* PS3 and *B. subtilis* WT (E102) and the E102A and E102A mutants (*B. subtilis*) structures are shown in Fig. 3B.

2.3. Mutations E102A/R in the ε subunit result in an increased ATP binding affinity

To examine whether engineering E102 to another residue influences the affinity of the ATP binding site, as our predictions would suggest, E102 was mutated to either an alanine (E102A) or an arginine (E102R). Detection of ATP binding kinetics was achieved in a manner as previously described by Kato-Yamada [38], where a single cysteine was introduced (Q107C) to allow labeling with Cy3 (see Fig. 4A).

The interaction between Cy3 and the adenosine ring of ATP creates a fluorescence enhancement effect [38]. Unfortunately, overexpression of WT *B. subtilis* epsilon E102 and the E102A, E102R mutants caused the formation of inclusion bodies, not an uncommon problem for this protein, so the purification method was based on that used for the ε subunit from *Spinacia oleracea* chloroplasts, which was also expressed as inclusion bodies [46]. During this purification method, the inclusion bodies were repeatedly washed with buffer containing 1% Triton X-100. Interestingly, SDS-PAGE analysis of the washes showed that each washing solution contained the ε subunit with high purity, an indicator of 'non-classical' inclusion bodies composed of folded protein [47]. After purification (Fig. 4B) WT *B. subtilis* ε subunit (E102), and the E102A,

E102R mutants were labeled with Cy3 *via* a maliamide linkage to the cysteine at position 107 (Fig. 4B, WT lanes 2 and 3; E102A lanes 4 and 5; E102R lanes 6 and 7). WT *B. subtilis* ε subunit (E102), and the E102A, E102R mutants lacking Q107C could not be labeled and after addition of ATP, showed no fluorescence change. Addition of ATP to Cy3-maleimide labeled WT *Bacillus subtilis* ε subunit (E102), and the E102A, E102R mutants resulted in an increase in fluorescence over time. In all experimental systems no further fluorescent change was observed if more than 4 mM ATP was used (Fig. 4C-E and S2A–C). For comparison with previous studies [23,24], any fluorescence enhancement at a given ATP concentration 220 s after the ATP injection was extracted for subsequent analysis (Fig. S7A–C). The resulting data was then plotted *versus* the ATP concentration and a hyperbolic binding curve fitted to the data (Fig. 4C-E). Under the conditions examined, the WT *Bacillus subtilis* ε subunit (E102) has a K_d for ATP of 1.8 mM (Fig. 4C and S2A), a figure similar to the previously measured K_d of 2.1 mM using NAM as a fluorophore [23]. Strikingly, when the E102A and E102R mutations were tested experimentally increased binding affinity values of 180 μM (~10 fold) and 33.3 μM (~54 fold) were measured for the E102A and E102R mutants respectively (Fig. 4C-E and S2A–C). This observation succinctly demonstrates that the MD simulations accurately predicted the role of E102 in tuning the affinity of the *Bacillus subtilis* ε subunit.

3. Discussion

Detailed biochemical and high-resolution structural information are essential to understanding ligand binding mechanisms in biomolecular complexes and rational enzyme design. Highly conserved sequence motifs are found in in a variety of proteins, which bind to the same ligand, such as *e.g.* ATP [2], GTP [48], or phosphate [49] binding motifs. This study reveals that analyzing the presence of such sequence motifs using simulations allows the accurate prediction of residues outside the active site that influence ligand binding, augmenting the efficiency of an enzyme, or this this example, biosensor design [50].

In this study, we show that the ligand binding site composition is not only influenced directly by the binding site residues but also potentially by allosteric effects caused by 'second shell' residues located in the vicinity of the binding site, clarifying the structural basis for ATP binding to the ε subunit of *Bacillus subtilis*, which differs with respect to the binding mode of the ε subunit from *Bacillus* PS3 [42,43]. Specifically, we used simulations to predict the existence of a salt bridge between an arginine (R99) and a glutamate (E102) residue in the ε subunit from *B. subtilis*. This interaction is not observed in the crystal structure of the ε subunit from *Bacillus* PS3 [42] or during MD simulations of the same subunit [43], and as a result, R99 was stably bound to ATP:Oγ [43]. The prediction of the E102–R99 salt bridge in *B. subtilis* is in agreement with previously reported experimental data, where the interaction with oppositely charged residues in the residue distance n (K/E)➔$n + 3$ (E/K) or n (K/E) ➔ $n + 4$ (E/K) was shown to be favorable and to stabilize α-helical structural elements [51–53]; this interaction cannot be formed in *Bacillus* PS3 due to the absence of E102 (R102).

To test our prediction that the rearrangement of the binding site residues results in a different ligand-binding mode, we computationally mutated the crucial residue (E102 in *B. subtilis*) to alanine or arginine (A and R respectively; R102 in *Bacillus* PS3). After introduction of these mutations we observed a rearrangement of R99 in both cases. R99 instead interacted with the ATP ligand, as observed for the ε subunit from *Bacillus* PS3 [42,43]. In addition, these mutations were tested experimentally, showing an increase of apparent binding affinity of 180 μM and 33.3 μM for the E102A and E102R mutants, respectively. These results confirm our simulations and are in agreement with previously conducted experiments (R99A mutation in *Bacillus* PS3) [24]. While we have shown here that a consequence of the reorientation of R99 in *B. subtilis*, the binding site structure of subunit ε, and consequently the ATP binding affinity is significantly modulated, an additional component of the decreased binding affinity is worthy of discussion. The
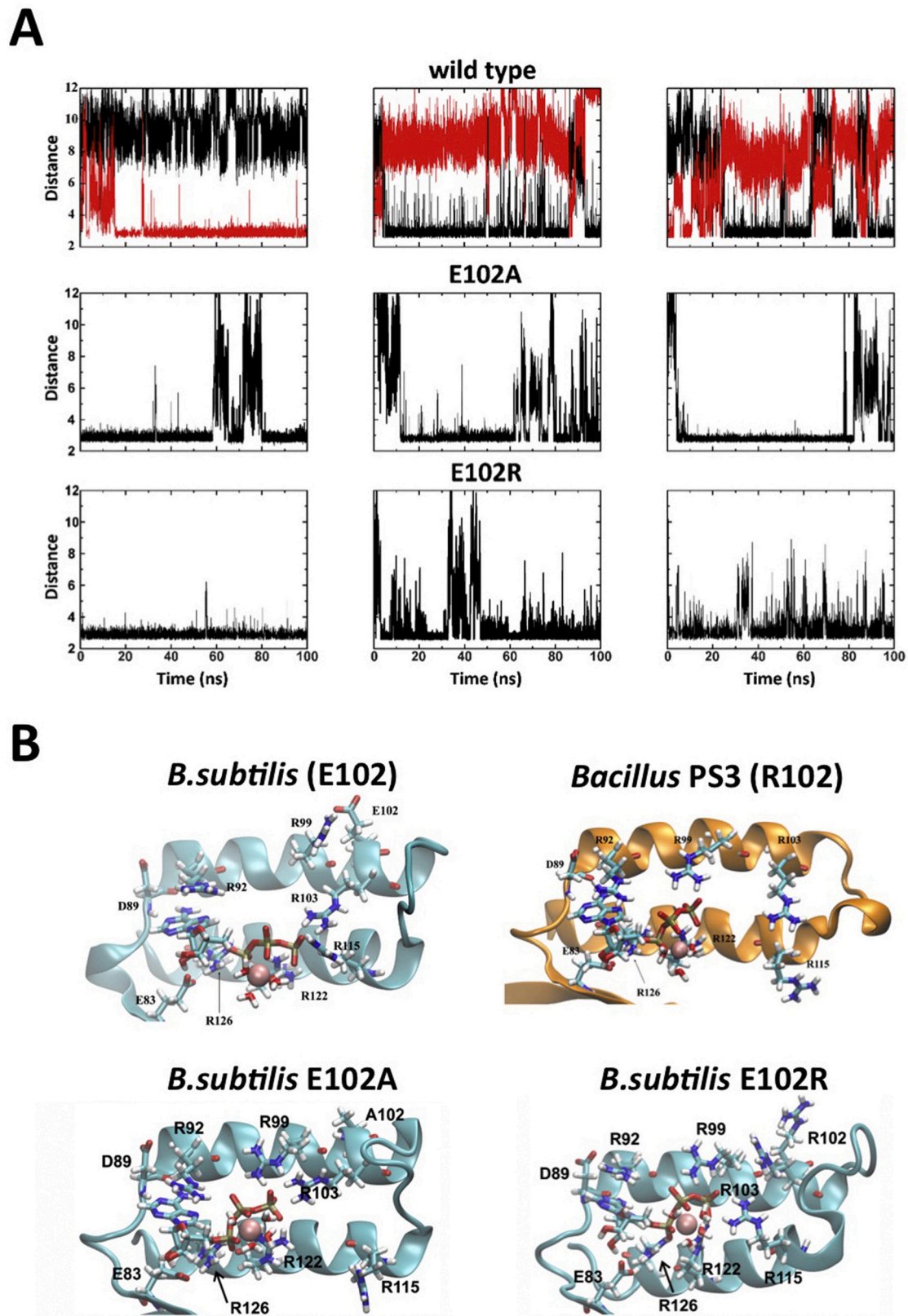
Fig. 3. Time-dependent minimum distance between residues E102, R99, and ATP in WT and predicted mutant structures of the *Bacillus subtilis* ε subunit. *A)* Upper 3 frames (left to right); the R99:NHx interaction with E102:Oεx (black) and R99:NHx with ATP:Oγ (red) WT *B. subtilis* ε subunit. Middle and Lower 3 frames (left to right); The interaction of R99:NHx with ATP:Oγ is shown for the E102A (middle 3 frames) and E102R *B. subtilis* ε subunit (lower 3 frames) mutants. All data were derived from three independent runs, each comprising 100 ns. Mg^{2+} is coordinated by ATP:Oα/Oβ in all simulations. *B)* Predicted ATP binding site structures of the WT *B. subtilis* ε subunit (E102), and the E102A, E102R mutants. Snapshot structures are shown for WT *B. subtilis* ε subunit (E102), *Bacillus* PS3 (adapted from [46]), *B. subtilis* ε subunit E102A, and E102R mutants. (For interpretation of the references to colour in this figure legend, the reader is referred to the web version of this article.)
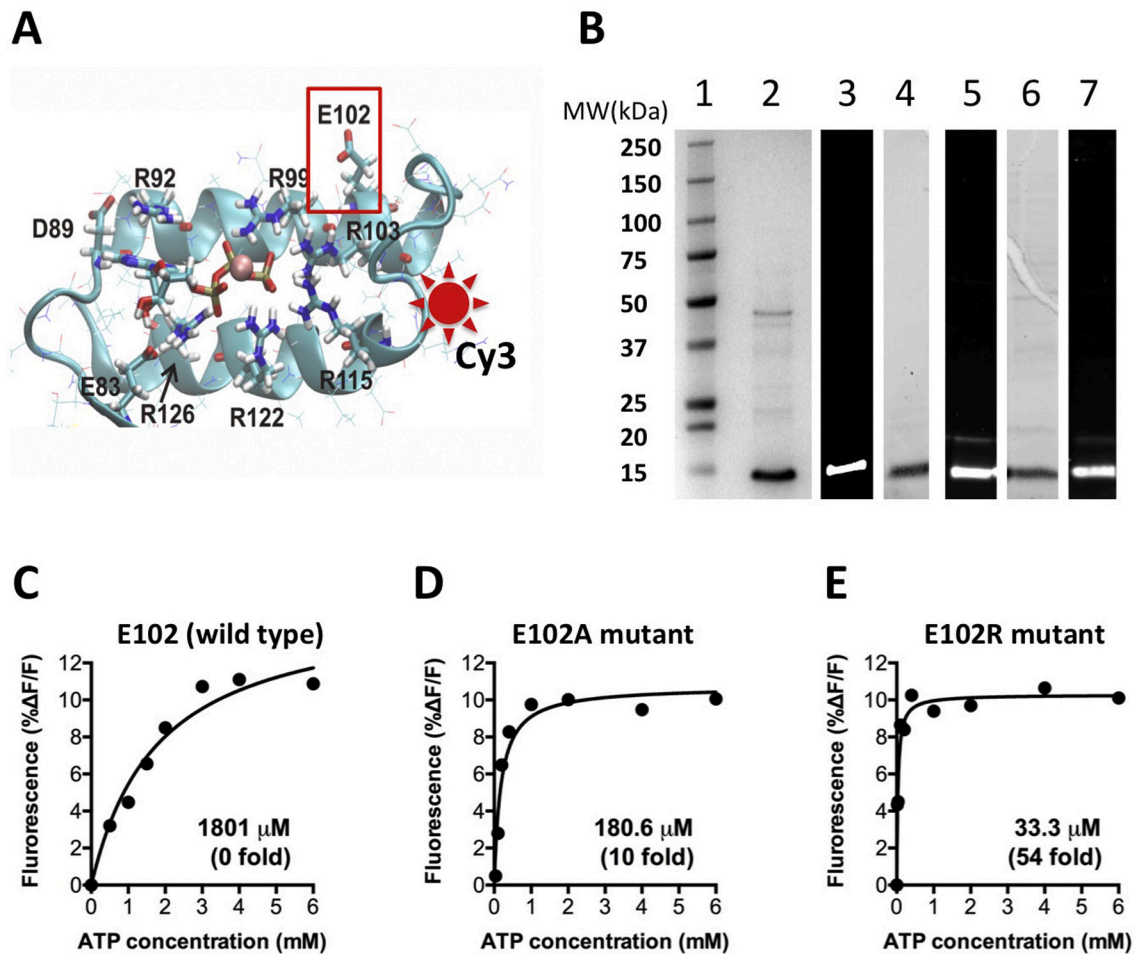
Fig. 4. Enhanced ATP binding *via* a single-site mutation at E102 in the *Bacillus subtilis* ε subunit. A, Depicts a Cy3-labeled annotated magnification of the WT *B. subtilis* ε subunit ATP binding site (E102). ATP, potential ATP binding residues and E102 are highlighted in licorice. The Mg^{2+} ion coordinating ATP is shown as a van der waal's sphere. Approximate Cy3 label location is indicated by a red star. B, SDS-PAGE analysis and labeling of Cy3 labeled WT *B. subtilis* ε subunit (E102), and the E102A, E102R mutants visualized under either white light (*Lanes 2, 4 and 6*) or using a Typhoon imaging system (GE Healthcare) with an excitation filter of 530 nm and an emission filter at 590 nm (*Lanes 3, 5 and 7*). *Lane 1*, Precision Plus Protein™ All Blue Prestained Protein Standards (Biorad)*; Lane 2–3,* 5 μg of WT *B. subtilis* ε subunit; *Lanes 4–5,* 5 μg of E102A*; Lanes 6–7,* 5 μg of E102A. The gel is visualized with SimplyBlue™ SafeStain. C-E, Change in fluorescence of Cy3 maleimide labeled WT *B. subtilis* ε subunit (E102), and the E102A, E102R mutants 220 s after ATP addition (also see Fig. S7A–C). A hyperbolic binding curve was fitted to the extracted data. Three experimental replicates were performed and the standard error of the mean is shown.

potential role allosteric Mg^{2+} binding site in *B. subtilis* [54], which is not present in the ε subunit from *Bacillus* PS3 [54], may also influence affinity. This predicted allosteric Mg^{2+} site (residues E59 and E86) has been proposed to be located at the hinge of the stable β-domain and the flexible α-helical motif, which undergoes the conformational change [54]. This conclusion is also supported by the R84A mutation in the ε subunit from *Bacillus* PS3, where R84 coordinates E86 and is thought to stabilize the contracted state of the protein [24,42]. Sequence alignment also supports the idea that this proposed allosteric ion-binding site is present in other organisms. Previous experiments show a ~ 500-fold lower affinity of the *B. subtilis* ε subunit compared to the *Bacillus* PS3 ε subunit, despite a 100% conserved ligand binding site ([23,24]: also see Fig. 1C). In support of this proposal, despite removal of the E102–R99 salt bridge, replacing it with *the very same residue* as found in position 102 in the *Bacillus* PS3 ε subunit (arginine), we were only to achieve a ~ 54-fold increase in affinity in the *B. subtilis* ε subunit E102R mutant. It is not inconceivable that the affinity difference between the E102A and E102R mutants is due to a repulsion effect, where E102R repeals R99 into twisting the helix to promote interaction with ATP, a phenomenon predicted by our MD simulations. The loss of the E102-R99 salt bridge due to the E102A mutation by comparison would only release R99, and not force the helix twist. Whether our hypotheses suggested here are

correct or not, clearly there is another affinity-tuning feature at work here outside the E102-R99 interaction.

While the effect of salt bridges stabilizing α-helical structures in peptides [52] and proteins [55] has been discussed previously, the role of the R99 – E102 salt bridge in the ε subunit from *Bacillus subtilis* is not obvious. This is evident by comparing the α-helical secondary structure of the ε subunit from *B. subtilis* with the ε subunits from *Escherichia coli* [56], *Bacillus* PS3 [42], *Thermosynechococcus elongates* BP-1 [57] or *Caldalkalibacillus thermarum* [44]. The salt bridge in question does not seem to be necessary to stabilize the α-helical structure of the ε subunit from *B. subtilis*, but as this study reveals, it serves to engineer the ATP binding affinity of the *B. subtilis* ε subunit to 2.1 mM [23]. Here, we propose a structure-function relationship where the salt bridge and an allosteric Mg^{2+} binding site [54] tune the ligand binding affinity of the ε subunit of F_1F_o ATP synthases in the low mM range, thus maintaining the required species-specific ATP concentration in the cell.

Interestingly, we found that this salt bridge is present in some organisms, but not others (Fig. 5 and Fig. S8). Taken in the context of the present study and the field of enzyme engineering, we can use our study to predict a reduced binding affinity to ATP for the ε subunit of *Bacillus cibi* or *Bacillus pumilus* compared to the ε subunit from *Bacillus* PS3. This is due to the presence of a glutamate in the vicinity of the binding site
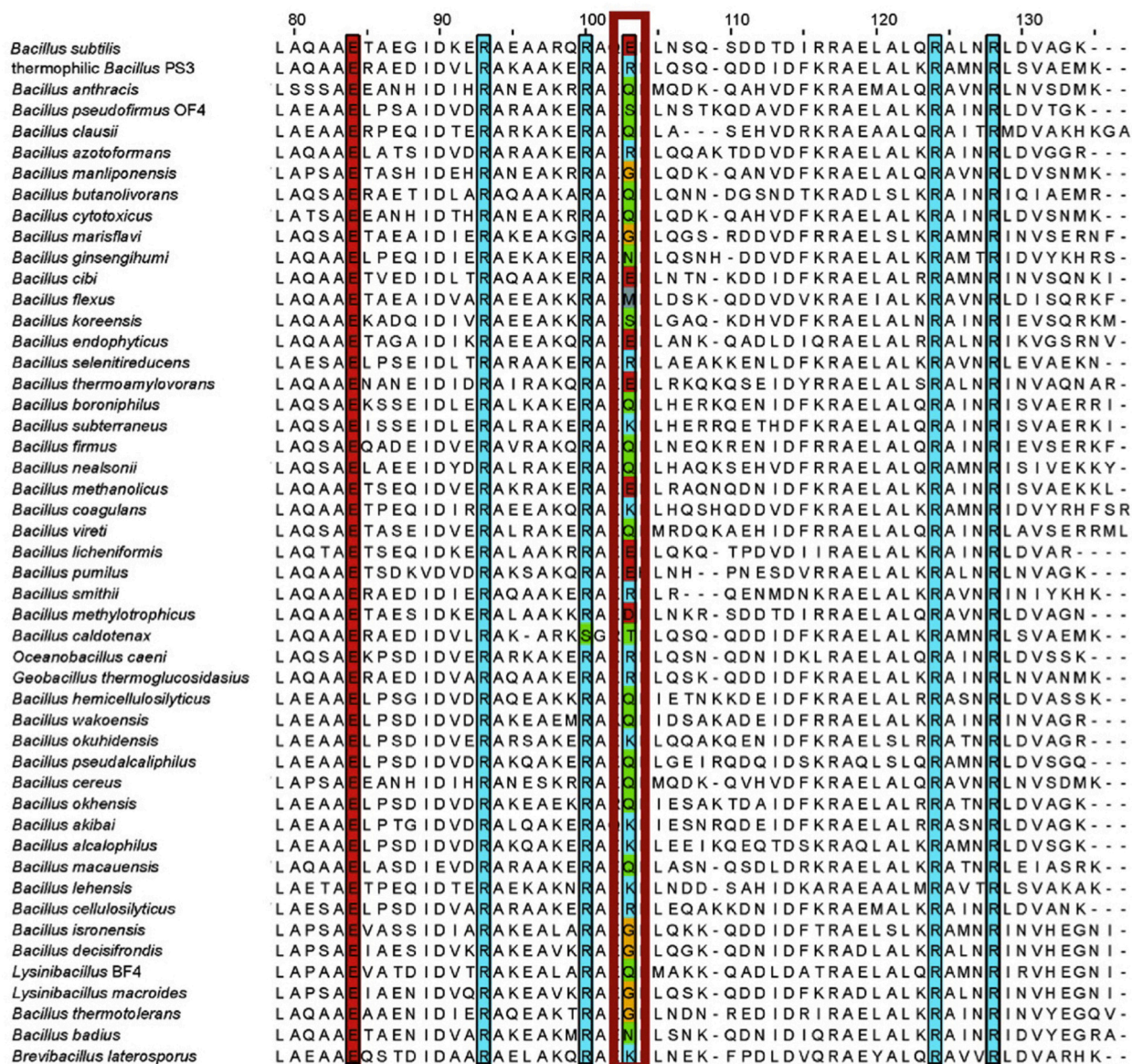
Fig. 5. Sequence alignment of the ε subunit from a variety of *Bacillus* sp. All ligand binding site residues are highlighted in colors according to charge (Blue = positive; Red = negative; Green = polar; neutral = orange (Gly) / blue-grey). The allostearic second shell residue E104 (*Bacillus subtilis* numbering) is marked by a red frame (position 103 in alignment). The alignment was generated with Jalview [58]. The full ε subunit sequence alignment can be found in Fig. S6. (For interpretation of the references to colour in this figure legend, the reader is referred to the web version of this article.)

(+3 residues upstream of the ligand-coordinating arginine), favoring formation of a salt bridge to displace the residues of opposed charge [53].

In summary, we have used MD simulations to predict the influence of a second-shell residue, outside a conserved binding site with 100% binding residue identity, yet having a 500-fold ATP affinity disparity, and engineered up to ~54-fold greater ATP binding affinity using a single point mutation.

In doing so, we have shown that the traditional enzyme engineering approach based on sequence alignment analysis may not necessarily predict the ligand binding mode although all binding residues are identical, even if the crystal structure of the same protein from a different organism indicates that the binding mode to the same ligand is conserved.

Collectively, this study also emphasizes that caution is required when interpreting ligand-protein binding based on homologous protein sequences. Lastly, this study serves as a simple prototype system

demonstrating the utility of using MD simulations combined with homology modeling for enzyme engineering, outlining a strategy for rational design of both specific therapeutic molecules for closely related members of protein families and enzymes with novel enzymatic function. However, while modeling methodologies such as MD are becoming ever more sophisticated, they are still not infallible, and certainly not a replacement for experimental verification. Having stated this, we expect our approach will find wide utility in fields such as biocatalysis to create enzymes with designed efficiencies towards industrially valuable products.

4. Material and methods

4.1. Molecular dynamics simulations

We used the simulated structural model following simulations from our previous studies [54], and modelled a Mg^{2+} ion between ATP:Oα/

Oβ. To summarize the model building approach used: We obtained the template sequence from the crystal structure of the ε subunit from *Bacillus* PS3 (PDB-ID: 2E5Y) and the target sequence *via* the uniprot database [59], and MODELLER was used to create a homology model [60]. The predicted structure of the resulting monomeric ε subunit from *Bacillus subtilis* was solvated in an octahedral box. We added 4 Mg^{2+} ions in total, with three of these placed in solution, and added additional counter ions to neutralize the overall system charge. The systems comprised in total ~ 41,000 atoms. The Mg^{2+} ion was modelled to ATP: Oα/Oβ, as shown earlier in the ε subunit from other organisms [43–45,61]. Simulations were performed for the *B. subtilis* WT protein and for *B. subtilis* E102A and E102R mutants. The mutations were built based on the homology model of the WT, only changing E102 to alanine or arginine using, while keeping all other residues constrained. The systems were first minimized for 2000 steps using the steepest descent integrator, followed by three independent unrestraint simulations for every system, for a total production time of 100 ns each. As we used the equilibrated structure from our previous work, we did not need to perform further equilibration. All simulations were performed using GROMACS (version 4.6.5) [62], with the AMBER-ILDN [63,64] force field. Mg^{2+} parameters were used as previously reported [65]. A constant pressure of 1 bar was maintained using the Parinello-Rahman barostat [66]. A constant temperature of 300 K was maintained using the velocity rescaling thermostat [67]. Periodic boundary conditions were applied in each dimension. Electrostatic interactions computed with the particle mesh Ewald (PME) method using a real space cut-off of 12 Å. Van der Waal's interactions were calculated using the same cut-off. The LINCS algorithm [68] was used to constrain all bonds connected to hydrogen atoms, and equations of motion were integrated using a time step of 2 fs. We applied internal GROMACS tools for the analysis of the trajectories; for the secondary structure analysis VMD was used [69].

4.2. Bacillus subtilis ε subunit mutagenesis

Bacillus subtilis ε subunit mutants containing the E102A and E102R mutations were made in a plasmid either already containing or lacking the Q107C mutation [23]. Complimentary primers (see Table S1) containing either the E102A and E102R mutations were used to introduce using the QuikChange method of full plasmid amplification (Stratagene). After mutagenesis *Dpn*I (New England Biolabs) was added to each sample to digest the parental plasmid for 2 h before heat inactivation and transformation into *E. coli* TOP10 cells.

4.3. Overexpression and purification

Escherichia coli BL21 (DE3) cells containing the plasmid encoding for the *Bacillus subtilis* ε wild type and subunit mutants were grown on 2× YT medium with 0.1 g/l ampicillin and 2 g/l glucose at 37 °C and 180 rpm. When an OD_{600} value of >0.5 was reached overexpression was induced by the addition of 0.2 mM isopropyl β-D-1-thiogalactopyranoside (IPTG, Thermo Fisher Scientific). The cultures were subsequently incubated for another 3 h at 37 °C and 180 rpm after which the cells were harvested by centrifuging at 9000 × *g* for 10 min. Each cell pellet was resuspended in 50 mM Tris/HCl (pH 7.5) buffer and again centrifuged at 9000 ×*g* for 10 min. Cell pellets were resuspended in lysis buffer containing 50 mM Tris/HCl (pH 7.5), 1 mM $MgCl_2$, 0.1 mM PMSF (phenylmethylsulfonyl fluoride, Sigma Aldrich), 0.1 mg/ml deoxyribonuclease I (Sigma Aldrich), and 1 mM fresh DTT (Sigma Aldrich) before lysis by three passages through a cell disruptor at 1.8 kbar (Constant Systems). The lysate was centrifuged at 9000 ×*g* for 10 min. The ε subunit was in inclusion bodies, so was resuspended in 20 ml 50 mM Tris/HCl (pH 7.5), 2 mM EDTA and 1 mM fresh DTT (buffer 1). The resulting pellet was resuspended and centrifuged at 9000 ×*g* for 10 min yielding soluble ε subunit in the supernatant. This wash step was repeated 5 times before the supernatant was concentrated with Amicon

Ultra 3 K filters (Merck) to a final volume of 200 μl. The ε subunit was then further purified with a Superdex 200 Increase 10/300 GL (GE Healthcare Life Sciences) size exclusion chromatography column with an NGC System (Biorad). The column was equilibrated with 10 mM Tris/HCl (pH 7.5), 2 mM EDTA and 140 mM NaCl (buffer 2) before sample was injected in the column. Thereafter, the column was eluted with 1.25 CV of buffer 2 supplemented with 1 mM DTT. Eluent fractions containing ε subunit were concentrated, frozen with liquid nitrogen and stored at −80 °C.

4.4. Protein determination and SDS-PAGE

Protein concentration was determined using the Bicinchoninic acid assay (Sigma) according to the manufacturers instructions with bovine serum albumin as a standard. Protein samples were analyzed with SDS-PAGE using 4–12% Criterion™ XT Bis-Tris Protein Gel then stained with SimplyBlue™ SafeStain (Invitrogen).

4.5. Fluorescent labelling of ε subunit

The *Bacillus subtilis* ε subunit was labeled by a marriage of two methods previously described [70,71], except Cy3 maleimide was used in place of biotin maleimide. The ε subunit sample was desalted with a centrifuge column (PD Minitrap™ G-25, GE Healthcare) equilibrated with 50 mM HEPES-NaOH (pH 6.5) and 100 mM NaCl by centrifuging at $1000 \times g$ for 2 min. TCEP was added in a 5:1 protein molar ratio and the sample incubated for 2 h at room temperature. Thereafter, Cy3 maleimide in dimethylsulfoxide (DMSO) was added in a 5:1 dye to protein molar ratio followed by incubation for 2 h at room temperature. Excess dye was removed with the same centrifuge column equilibrated with 50 mM HEPES-KOH (pH 7.5), 100 mM KCl, 10 mM $MgCl_2$. Labeling was subsequently analyzed by SDS-PAGE and Cy3 maleimide labeling detected by imaging the unstained gel with an Amersham Typhoon Imaging System (GE Healthcare). Gels were subsequently stained with SimplyBlue™ SafeStain (Invitrogen).

4.6. ATP binding assays

Fluorescence was measured with a Synergy 2 Microplate Reader (Biotek) using a black microplate (Greiner). To measure Cy3 maleimide fluorescence, an excitation filter of 530 nm with a 25 nm bandwidth and an emission filter at 590 nm with a 35 nm bandwidth were used at 22 °C. Each reaction mixture contained 100 μl of 820 nM labeled ε subunit in 50 mM HEPES–KOH (pH 7.5), 100 mM KCl and 10 mM $MgCl_2$ and more buffer was added such that a final volume of 200 μl is obtained after the addition of ATP. Fluorescence was measured for 30–60 s at 1.66 Hz followed by an injection of concentrated ATP in the same buffer into the sample resulting in a final volume of 200 μl. This resulted in a final labeled ε subunit concentration of 410 nM. Fluorescence was subsequently measured for another 6 min at 1.66 Hz.

Author statement

AK and DGGM conceptualized the study. AK conceptualization, investigation, analysis, writing. AK, PJB, BvdH, KCCK, LM, FT and DGGM contributed to the investigation and formal analysis. AK and DGGM wrote the manuscript original draft and conducted the reviewing and editing.

Declaration of Competing Interest

We declare that we have no competing financial interests or otherwise.

Acknowledgements

Appendix A. Supplementary data

Supplementary data to this article can be found online at https://doi.org/10.1016/j.bbagen.2020.129766.

References

[1] P.A. Lambert, Bacterial resistance to antibiotics: modified target sites, Adv. Drug Deliv. Rev. 57 (10) (2005) 1471–1485.

[2] J.E. Walker, M. Saraste, M. Runswick, N.J. Gay, Distantly related sequences in the alpha- and beta-subunits of ATP synthase, myosin, kinases and other ATP-requiring enzymes and a common nucleotide binding fold, EMBO J. 1 (8) (1982) 945–951.

[3] S. Arai, et al., Rotation mechanism of *Enterococcus hirae* V1-ATPase based on asymmetric crystal structures, Nature 493 (7434) (2013) 703–707.

[4] S. Zimmermann, S. Pfenning, P. Neumann, H. Yonus, U. Weininger, M. Kovermann, J. Balbach, M.T. Stubbs, High-resolution structures of the D-alanyl carrier protein (Dcp) DltC from Bacillus subtilis reveal equivalent conformations of apo - and holo -forms, FEBS Lett. 589 (18) (2015) 2283–2289.

[5] J.K. Hakulinen, J. Hering, G. Branden, H. Chen, A. Snijder, M. Ek, P. Johansson, MraY–antibiotic complex reveals details of tunicamycin mode of action, Nat. Chem. Biol. 13 (3) (2017) 265–267.

[6] J. Danielsson, R. Pierattelli, L. Banci, A. Gräslund, High-resolution NMR studies of the zinc-binding site of the Alzheimer's amyloid β-peptide, FEBS J. 274 (1) (2007) 46–59.

[7] A. Merk, et al., Breaking Cryo-EM resolution barriers to facilitate drug discovery, Cell. 165 (7) (2016) 1698–1707.

[8] H. Guo, G.M. Courbon, S.A. Bueler, J. Mai, J. Liu, J.L. Rubenstein, Structure of the mycobacterial ATP synthase with the TB drug bedaquiline, bioRxiv (2020), https://doi.org/10.1101/2020.08.06.225375.

[9] C. He, L. Preiss, B. Wang, L. Fu, H. Wen, X. Zhang, H. Cui, T. Meier, D. Yin, Structural simplification of bedaquiline: the discovery of 3-(4-(N, N -dimethylaminomethyl)phenyl)quinoline-derived antitubercular lead compounds, ChemMedChem 12 (2) (2017) 106–119.

[10] A.C. Anderson, The process of structure-based drug design, Chem. Biol. 10 (9) (2003) 787–797.

[11] S.B.J. Kan, R.D. Lewis, K. Chen, F.H. Arnold, Directed evolution of cytochrome c for carbon-silicon bond formation: bringing silicon to life, Science 354 (6315) (2016) 1048–1051.

[12] H. Imamura, K.P. Huynh Nhat, H. Togawa, K. Saito, R. Iino, Y. Kato-Yamada, T. Nagai, H. Noji, Visualization of ATP levels inside single living cells with fluorescence resonance energy transfer-based genetically encoded indicators, Proc. Natl. Acad. Sci. U. S. A. 106 (37) (2009) 15651–15656.

[13] M. Luo, W. Zhao, H. Patel, A.P. Srivastava, J. Symersky, M.M. Bonar, J.D. Faraldo-Gomez, M. Liao, D.M. Mueller, Bedaquiline inhibits the yeast and human mitochondrial ATP synthases, Commun. Biol. 3 (2020) 452, https://doi.org/10.1038/s42003-020-01173-z.

[14] K. Hards, D.G.G. McMillan, L.A. Schurig-Briccio, R.B. Gennis, H. Lill, D. Bald, G.M. Cook, Ionophoric effects of the antitubercular drug bedaquiline, Proc. Natl. Acad. Sci. U. S. A. 115 (2018) 7326–7331.

[15] I.M. Kapetanovic, Computer-aided drug discovery and development (CADDD): in silico-chemico-biological approach, Chem. Biol. Interact. 171 (2) (2008) 165–176.

[16] M.J. Keiser, et al., Predicting new molecular targets for known drugs, Nature 462 (7270) (2009) 175–181.

[17] M.J. Keiser, B.L. Roth, B.N. Armbruster, P. Ernsberger, J.J. Irwin, B.K. Shoichet, Relating protein pharmacology by ligand chemistry, Nat. Biotechnol. 25 (2) (2007) 197–206.

[18] O. Lichtarge, H.R. Bourne, F.E. Cohen, An evolutionary trace method defines binding surfaces common to protein families, J. Mol. Biol. 257 (2) (1996) 342–358.

[19] M. Weisel, E. Proschak, G. Schneider, PocketPicker: analysis of ligand binding-sites with shape descriptors, Chem. Cent. J. 1 (1) (2007) 7.

[20] A. Brakoulias, R.M. Jackson, Towards a structural classification of phosphate binding sites in protein-nucleotide complexes: an automated all-against-all

[21] structural comparison using geometric matching, Proteins. Struct. Funct. Bioinforma. 56 (2) (2004) 250–260.

[21] A.A. Lee, M.P. Brenner, L.J. Colwell, Predicting protein-ligand affinity with a random matrix framework, Proc. Natl. Acad. Sci. U. S. A. 113 (48) (2016) 13564–13569.

[22] T. Liu, R.B. Altman, Using multiple microenvironments to find similar ligand-binding sites: application to kinase inhibitor binding, PLoS Comput. Biol. 7 (12) (2011), e1002326.

[23] Y. Kato-Yamada, Isolated ε subunit of Bacillus subtilis F1-ATPase binds ATP, FEBS Lett. 579 (30) (2005) 6875–6878.

[24] S. Kato, M. Yoshida, Y. Kato-Yamada, Role of the ε subunit of thermophilic F1-ATPase as a sensor for ATP, J. Biol. Chem. 282 (52) (2007) 37618–37623.

[25] A. Krah, U. Zachariae, Insights into the ion-coupling mechanism in the MATE transporter NorM-VC, Phys. Biol. 14 (4) (2017).

[26] A. Krah, R.G. Huber, U. Zachariae, P.J. Bond, On the ion coupling mechanism of the MATE transporter ClbM, Biochim. Biophys. Acta Biomembr. 1862 (2) (2020) 1–9.

[27] A. Krah, J.K. Marzinek, P.J. Bond, Characterizing the hydration properties of proton binding sites in the ATP synthase c-rings of Bacillus species, J. Phys. Chem. B 124 (2020) 7176–7183.

[28] R.G. Huber, H. Fan, P.J. Bond, The structural basis for activation and inhibition of ZAP-70 kinase domain, PLoS Comput. Biol. 11 (10) (2015), e1004560.

[29] M. Prieß, L.V. Schäfer, Release of entropic spring reveals conformational coupling mechanism in the ABC transporter BtuCD-F, Biophys. J. 110 (11) (2016) 2407–2418.

[30] A. Krah, R.G. Huber, P.J. Bond, How ligand binding affects the dynamical transition temperature in proteins, ChemPhysChem (2020), https://doi.org/10.1002/cphc.201901221.

[31] X.-Q. Yao, H. Kenzaki, S. Murakami, S. Takada, Drug export and allosteric coupling in a multidrug transporter revealed by molecular simulations, Nat. Commun. 1 (8) (2010) 117.

[32] X.-Q. Yao, N. Kimura, S. Murakami, S. Takada, Drug uptake pathways of multidrug transporter AcrB studied by molecular simulations and site-directed mutagenesis experiments, J. Am. Chem. Soc. 135 (20) (2013) 7474–7485.

[33] T. Paramo, A. East, D. Garzón, M.B. Ulmschneider, P.J. Bond, Efficient characterization of protein cavities within molecular simulation trajectories: trj_cavity, J. Chem. Theory Comput. 10 (5) (2014) 2151–2164.

[34] D.T. Baptista-Hon, A. Krah, U. Zachariae, T.G. Hales, A role for loop G in the β1 strand in GABA A receptor activation, J. Physiol. 594 (19) (2016) 5555–5571.

[35] N. Homeyer, F. Stoll, A. Hillisch, H. Gohlke, Binding free energy calculations for lead optimization: assessment of their accuracy in an industrial drug design context, J. Chem. Theory Comput. 10 (8) (2014) 3331–3344.

[36] L. Wang, et al., Accurate and reliable prediction of relative ligand binding potency in prospective drug discovery by way of a modern free-energy calculation protocol and force field, J. Am. Chem. Soc. 137 (7) (2015) 2695–2703.

[37] A. Krah, R.G. Huber, D.G.G. McMillan, P.J. Bond, The molecular basis for purine binding selectivity in the bacterial ATP synthase ε subunit, ChemBioChem (2020), cbic.202000291, https://doi.org/10.1002/cbic.202000291.

[38] Y. Kato-Yamada, High affinity nucleotide-binding mutant of the ε subunit of thermophilic F1-ATPase, Biochem. Biophys. Res. Commun. 469 (2016) 1129–1132.

[39] A. Krah, Linking structural features from mitochondrial and bacterial F-type ATP synthases to their distinct mechanisms of ATPase inhibition, Prog. Biophys. Mol. Biol. 119 (1) (2015) 94–102.

[40] A. Krah, M. Zarco-Zavala, D.G.G. McMillan, Insights into the regulatory function of the ε subunit from bacterial F-type ATP synthases: a comparison of structural, biochemical and biophysical data, Open Biol. 8 (5) (2018), 170275.

[41] M. Sobti, R. Ishmukhametov, J.C. Bouwer, A. Ayer, C. Suarna, N.J. Smith, M. Christie, R. Stocker, T.M. Duncan, A.G. Stewart, Cryo-EM reveals distinct conformations of E coli ATP synthase on exposure to ATP, Elife 8 (2019), e43864.

[42] H. Yagi, N. Kajiwara, H. Tanaka, T. Tsukihara, Y. Kato-Yamada, M. Yoshida, H. Akutsu, Structures of the thermophilic F1-ATPase subunit suggesting ATP-regulated arm motion of its C-terminal domain in F1, Proc. Natl. Acad. Sci. U. S. A. 104 (27) (2007) 11233–11238.

[43] A. Krah, S. Takada, On the ATP binding site of the ε subunit from bacterial F-type ATP synthases, Biochim. Biophys. Acta Bioenerg. 1857 (4) (2016) 332–340.

[44] S.A. Ferguson, G.M. Cook, M.G. Montgomery, A.G.W. Leslie, J.E. Walker, Regulation of the thermoalkaliphilic F1-ATPase from Caldalkalibacillus thermarum, Proc. Natl. Acad. Sci. U. S. A. 113 (39) (2016) 10860–10865.

[45] A. Krah, Y. Kato-Yamada, S. Takada, The structural basis of a high affinity ATP binding ε subunit from a bacterial ATP synthase, PLoS One 12 (5) (2017), e0177907.

[46] Y. Kato-Yamada, M. Yoshida, Isolated epsilon subunit of thermophilic F1-ATPase binds ATP, J. Biol. Chem. 278 (38) (2003) 36013–36016.

[47] S. Jevševar, V. Gaberc-Porekar, I. Fonda, B. Podobnik, J. Grdadolnik, V. Menart, Production of nonclassical inclusion bodies from which correctly folded protein can be extracted, Biotechnol. Prog. 21 (2) (2005) 632–639.

[48] T.E. Dever, M.J. Glynias, W.C. Merrick, GTP-binding domain: three consensus sequence elements with distinct spacing, Proc. Natl. Acad. Sci. U. S. A. 84 (7) (1987) 1814–1818.

[49] A.K.H. Hirsch, F.R. Fischer, F. Diederich, Phosphate recognition in structural biology, Angew. Chem. Int Ed. 46 (3) (2007) 338–352.

[50] O. Lichtarge, M.E. Sowa, Evolutionary predictions of binding surfaces and interactions, Curr. Opin. Struct. Biol. 12 (1) (2002) 21–27.

[51] J.M. Scholtz, H. Qian, V.H. Robbins, R.L. Baldwin, The energetics of ion-pair and hydrogen-bonding interactions in a helical peptide, Biochemistry. 32 (37) (1993) 9668–9676.

[50] L. Mayne, S. Englander, R. Qiu, J. Yang, Y. Gong, E.J. Spek, N.R. Kallenbach, Stabilizing effect of a multiple salt bridge in a prenucleated peptide, J. Am. Chem. Soc. 120 (41) (1998) 10643–10645.

[53] E.G. Baker, G.J. Bartlett, M.P. Crump, R.B. Sessions, N. Linden, C.F.J. Faul, D. N. Woolfston, Local and macroscopic electrostatic interactions in single α-helices, Nat. Chem. Biol. 11 (3) (2015) 221.

[54] A. Krah, S. Takada, On the Mg^{2+} binding site of the ε subunit from bacterial F-type ATP synthases, Biochim. Biophys. Acta Bioenerg. 1847 (10) (2015) 1101–1112.

[55] K. Yip, T.J. Stillman, K.L. Britton, P.J. Artymiuk, P.J. Baker, S.E. Sedelnikova, P. C. Engel, A. Pasquo, R. Chiaraluce, V. Consalvi, R. Scandurra, D.W. Rice, The structure of Pyrococcus furiosus glutamate dehydrogenase reveals a key role for ion-pair networks in maintaining enzyme stability at extreme temperatures, Structure 3 (11) (1995) 1147–1158.

[56] U. Uhlin, G.B. Cox, J.M. Guss, Crystal structure of the epsilon subunit of the proton-translocating ATP synthase from Escherichia coli, Structure 5 (9) (1997) 1219–1230.

[57] H. Yagi, H. Konno, T. Murakami-Fuse, A. Isu, T. Oroguchi, H. Akutsu, M. Ikeeguchi, T. Hisabori, Structural and functional analysis of the intrinsic inhibitor subunit ε of F1 -ATPase from photosynthetic organisms, Biochem. J. 425 (1) (2010) 85–98.

[58] A.M. Waterhouse, J.B. Procter, D.M.A. Martin, M. Clamp, G.J. Barton, Jalview Version 2-a multiple sequence alignment editor and analysis workbench, Bioinformatics 25 (9) (2009) 1189–1191.

[59] The UniProt Consortium, UniProt: the universal protein knowledgebase, Nucleic Acids Res. 45 (D1) (2017) D158–D169, https://doi.org/10.1093/nar/gkw1099.

[60] A. Fiser, A. Šali, Modeller: generation and refinement of homology-based protein structure models, Methods Enzymol. 374 (2003) 461–491.

[61] A. Krah, P.J. Bond, Single mutations in the ε subunit from thermophilic Bacillus PS3 generate a high binding affinity site for ATP, PeerJ 6 (2018) e5505.

[62] S. Pronk, S. Pall, R. Schultz, P. Larsson, P. Bjelkmar, R. Apostolov, M.R. Shirts, J. C. Smith, P.M. Kasson, D. van der Spoel, B. Hess, E. Lindahl, GROMACS 4.5: a high-throughput and highly parallel open source molecular simulation toolkit, Bioinformatics 29 (7) (2013) 845–854.

[63] W.D. Cornell, P. Cieplak, C.I. Bayly, I.R. Gould, K.M. Merz, D.M. Ferguson, D. C. Spellmeyer, T. Fox, J.W. Caldwell, P.A. Kollman, A second generation force field for the simulation of proteins, nucleic acids, and organic molecules, J. Am. Chem. Soc. 117 (19) (1995) 5179–5197.

[64] K.L. Meagher, L.T. Redman, H.A. Carlson, Development of polyphosphate parameters for use with the AMBER force field, J. Comput. Chem. 24 (9) (2003) 1016–1025.

[65] J. Åqvist, Ion-water interaction potentials derived from free energy perturbation simulations, J. Phys. Chem. 94 (21) (1990) 8021–8024.

[66] M. Parrinello, A. Rahman, Polymorphic transitions in single crystals: a new molecular dynamics method, J. Appl. Phys. 52 (12) (1981) 7182–7190.

[67] G. Bussi, D. Donadio, M. Parrinello, Canonical sampling through velocity rescaling, J. Chem. Phys. 126 (1) (2007) 014101.

[68] B. Hess, H. Bekker, H.J.C. Berendsen, J.G.E.M. Fraaije, LINCS: a linear constraint solver for molecular simulations, J. Comput. Chem. 18 (12) (1997) 1463–1472.

[69] W. Humphrey, A. Dalke, K. Schulten, VMD: visual molecular dynamics, J. Mol. Graph. 14 (1996) 33–38.

[70] M.R. Cheetham, J.P. Bramble, D.G.G. McMillan, L. Krzeminski, X. Han, B.R. G. Johnson, R.J. Bushby, P.D. Olmsted, L.J.C. Jeuken, S.J. Marritt, J.N. Butt, S. D. Evans, Concentrating membrane proteins using asymmetric traps and AC electric fields, J. Am. Chem. Soc. 133 (17) (2011) 6521–6524.

[71] D.G.G. McMillan, R. Watanabe, H. Ueno, G.M. Cook, H. Noji, Biophysical characterization of a thermoalkaliphilic molecular motor with a high stepping torque gives insight into evolutionary ATP synthase adaptation, J. Biol. Chem. 291 (46) (2016) 23965–23977.